---

**Article:**
Saunders, L.C., Eaden, J.A., Bianchi, S.M. et al. (2020) Free breathing lung T1 mapping using image registration in patients with idiopathic pulmonary fibrosis. Magnetic Resonance in Medicine, 84 (6). pp. 3088-3102. ISSN: 0740-3194

https://doi.org/10.1002/mrm.28342

---

Received: 9 December 2019 | Revised: 4 May 2020 | Accepted: 13 May 2020

DOI: 10.1002/mrm.28342

FULL PAPER

Magnetic Resonance in Medicine

# Free breathing lung $T_1$ mapping using image registration in patients with idiopathic pulmonary fibrosis

**Laura C. Saunders**[1] | **James A. Eaden**[1] | **Stephen M. Bianchi**[2] | **Andrew J. Swift**[1] | **Jim M. Wild**[1]

[1]POLARIS, Imaging Sciences, Department of IICD, University of Sheffield, Sheffield, United Kingdom

[2]Academic Directorate of Respiratory Medicine, Sheffield Teaching Hospitals NHS Foundation Trust, Sheffield, United Kingdom

**Correspondence**
Jim M. Wild, POLARIS, Imaging Sciences, C Floor, Royal Hallamshire Hospital, University of Sheffield, Sheffield, S10 2JF, United Kingdom.
Email: j.m.wild@sheffield.ac.uk

**Funding information**
This work was supported by MRC grant MR/M008894/1 and the Wellcome Trust 205188/Z/16/Z

**Purpose:** To assess the use of image registration for correcting respiratory motion in free breathing lung $T_1$ mapping acquisition in patients with idiopathic pulmonary fibrosis (IPF).

**Theory and Methods:** The method presented used image registration to synthetic images during postprocessing to remove respiratory motion. Synthetic images were generated from a model of the inversion recovery signal of the acquired images that incorporated a periodic lung motion model. Ten healthy volunteers and 19 patients with IPF underwent 2D Look-Locker $T_1$ mapping acquisition at 1.5T during inspiratory breath-hold and free breathing. Eight healthy volunteers and seven patients with IPF underwent $T_1$ mapping acquisition during expiratory breath-hold. Fourteen patients had follow-up scanning at 6 months. Dice similarity coefficient (DSC) was used to evaluate registration efficacy.

**Results:** Image registration increased image DSC ($P < .001$) in the free breathing inversion recovery images. Lung $T_1$ measured during a free breathing acquisition was lower in patients with IPF when compared with healthy controls (inspiration: $P = .238$; expiration: $P = .261$; free breathing: $P = .021$). Measured lung $T_1$ was higher in expiration breath-hold than inspiration breath-hold in healthy volunteers ($P < .001$) but not in patients with IPF ($P = .645$). There were no other significant differences between lung $T_1$ values within subject groups.

**Conclusions:** The registration technique significantly reduced motion in the Look-Locker images acquired during free breathing and may improve the robustness of lung $T_1$ mapping in patients who struggle to hold their breath. Lung $T_1$ measured during a free breathing acquisition was significantly lower in patients with IPF when compared with healthy controls.

**KEYWORDS**
diffuse lung disease, image registration, Lung, motion correction, $T_1$ map

## 1 | INTRODUCTION

Parametric lung $T_1$ (longitudinal relaxation time) mapping has the potential to characterize pathophysiological changes in the tissue of the lung.[1] Idiopathic pulmonary fibrosis (IPF) is a progressive lung condition where fibrosis occurs within heterogeneous regions of the lung, resulting in alveolar-capillary gas exchange limitation, decreased lung volume, and reduced function of the lung. $T_1$ mapping may be able to characterize regional tissue changes within the lung[2] and in combination with oxygen enhancement can demonstrate regions of poor ventilation and perfusion matching.[3,4] Therefore, $T_1$ mapping may be able to assist in diagnosing and characterizing the rate of deterioration of the lungs of patients with IPF without the use of invasive biopsy or ionizing radiation. This is particularly pertinent in IPF as the established pulmonary function tests (functional vital capacity and carbon monoxide diffusing capacity) have limited sensitivity to longitudinal pathophysiological changes and limited prognostic value.[5] Previous studies by Stadler et al at 1.5T in patients with IPF using a 2D inversion recovery gradient echo Look-Locker approach, have shown a mean lung $T_1$ of 1.00 ± 0.10 s at inspiration and 1.28 ± 0.17 s at expiration (echo time [TE] = 1.4 ms).[1] Healthy volunteers have been shown to have a mean $T_1$ of 1.12 ± 0.12 s at inspiration and 1.33 ± 0.17 s at expiration (TE = 1.4 ms)[6] using the same sequence. The work of Mirsadraee et al at 3T, using a steady state sampled MOLLI sequence has shown fibrotic regions of the lung to have a significantly higher $T_1$ than non-fibrotic regions of the lung.[2] The differences seen between lung $T_1$ in IPF in the studies by Stadler et al and Mirsadraee et al may be due to the changes to $T_1$ values in lung tissue, blood and fibrosis with field strength, the different contrast weighting of the sequences used to map $T_1$ and variation in region of interest placement. Therefore, further work is needed at both field strengths to establish the pattern of changes in lung $T_1$ in patients with IPF.

Patients with respiratory disease such as IPF, experience breathlessness and may, therefore, struggle to maintain breath-holds, and may demonstrate diaphragmatic drift throughout imaging leading to inaccuracies in the resultant lung $T_1$ maps. Navigated free breathing acquisitions can be used to circumvent the acquisition time restriction of a breath-hold and allow free breathing lung $T_1$ mapping and can also permit simultaneous $T_2^*$ mapping and 3D data acquisition.[7,8] However, scan efficiency is reduced as only a fraction of the scan time is used for image acquisition, and this reduces clinical utility considerably. In addition, there may still be some misregistration between images acquired in this manner if the acquisition window is large. Whole lung $T_1$ is also known to be dependent on lung inflation[6] and free breathing occurs at tidal volume, whereas inspiratory and expiratory breath-holds occur within the inspiratory and expiratory reserve. Therefore, free breathing lung $T_1$ values may be expected to fall between inspiratory and expiratory breath-hold values. However, small changes in the oxy/deoxhemoglobin concentration due to breath-hold may also result in differences in blood $T_1$ (and, therefore, whole lung $T_1$) when acquired during breath-hold and free breathing.

A fast, efficient method for free breathing lung $T_1$ mapping may improve patient comfort, by removing the need for breath-hold and reducing the time the patient is on the MRI scanner, and also improve $T_1$ accuracy, by reducing misregistration in cases where patients' breath-hold drifts. Look-Locker inversion recovery imaging is a fast and efficient method of single-slice $T_1$ mapping, which generally requires a breath-hold for the duration of 16 image acquisitions with different inversion time which typically lasts 7 seconds.[9] Using image registration during postprocessing to correct for motion in lung $T_1$ mapping images would allow for efficient and comfortable lung $T_1$ mapping. To acquire multiple breath-hold Look-Locker slices, additional time is needed for the patient to recover from the breath-holds. However, with a registered free breathing approach, this additional time could be removed resulting in faster multi-slice acquisition.

Image registration between Look-Locker images is challenging due to considerable changes in image contrast between images acquired at different inversion times (Ti), which is caused by the different relaxation times ($T_1$) of the tissues within the image. When registering inversion recovery images using a simple frame-to-frame registration the contrast differences at each Ti could result in registration errors, as demonstrated in cardiac inversion recovery MOLLI images by both Xue at al,[10] who compared frame-to-frame registration to a non-rigid registration algorithm using the local cross-correlation as the similarity metric and Tao et al,[11] who compared frame-to-frame registration to a non-rigid registration algorithm with a mutual-informational based similarity metric.

One method to overcome the current image registration limitations caused by the contrast differences in acquired images is to use a data-driven signal model to create synthetic images. Synthetic image based registration techniques have been used successfully in dynamic contrast enhanced MRI in the body[12-15] as well as in cardiac $T_1$ mapping images.[10,16] However, these methods have not yet been applied to lung $T_1$ mapping. In this work, a synthetic image based registration method for motion correction is presented to allow free breathing lung $T_1$ mapping using a conventional 2D Look-Locker acquisition sequence. The method is evaluated, alongside breath-hold $T_1$ mapping with the same sequence in patients with IPF and healthy subjects.

## 2 | THEORY

The method presented uses two key techniques: (1) a combined respiratory and inversion recovery signal model (CRIR) to select three spatially aligned acquired images; (2) a simplified inversion recovery model to produce synthetic images for image registration, using those three selected spatially aligned images. Acquired images are then co-registered to the synthetic images, and then, used to calculate a registered $T_1$ map. A schematic work flow and explanation of the steps is presented in Figure 1.

### 2.1 | Simplified inversion recovery model

The relaxation model used to compute the synthetic images is adapted from a method developed for cardiac inversion recovery MR images which uses a two parameter model (see Equation 1), a manual cardiac segmentation and undergoes iterative improvement of the synthetic images.[16]

$$S(t) = A(1 - 2e^{-t/T_1^*}) \quad (1)$$

where S is signal, t is time, and A and $T_1^*$ are parameters to be fit.

The approach implemented in our work does not require a segmentation and uses a single parameter model (see Equation 2) where the third image input into the model ($S_{t3}$ which is determined using the CRIR model, see Figure 1 "Data-driven image selection") is used as a surrogate for a fully recovered image. This provides a more robust initial fit and removes the necessity of time-costly iterations and manual segmentation.

$$S(t) = S_{t3}(1 - 2e^{-t/T_1^*}). \quad (2)$$

Three spatially aligned images (alignment assessed on diaphragmatic position) are input into the synthetic image model (Equation 2) and a non-rigid pair-wise image registration between the synthetic images and the corresponding acquired images is performed.

For this method to be applicable for free breathing acquisitions, an algorithm automatically selects images with a similar respiratory state from the free breathing acquisition by fitting the image data to the CRIR model. The model is based upon the concept that the total signal from a fixed region of interest (ROI) in the body will be effected by both the inversion recovery behavior of the protons in this region of tissue

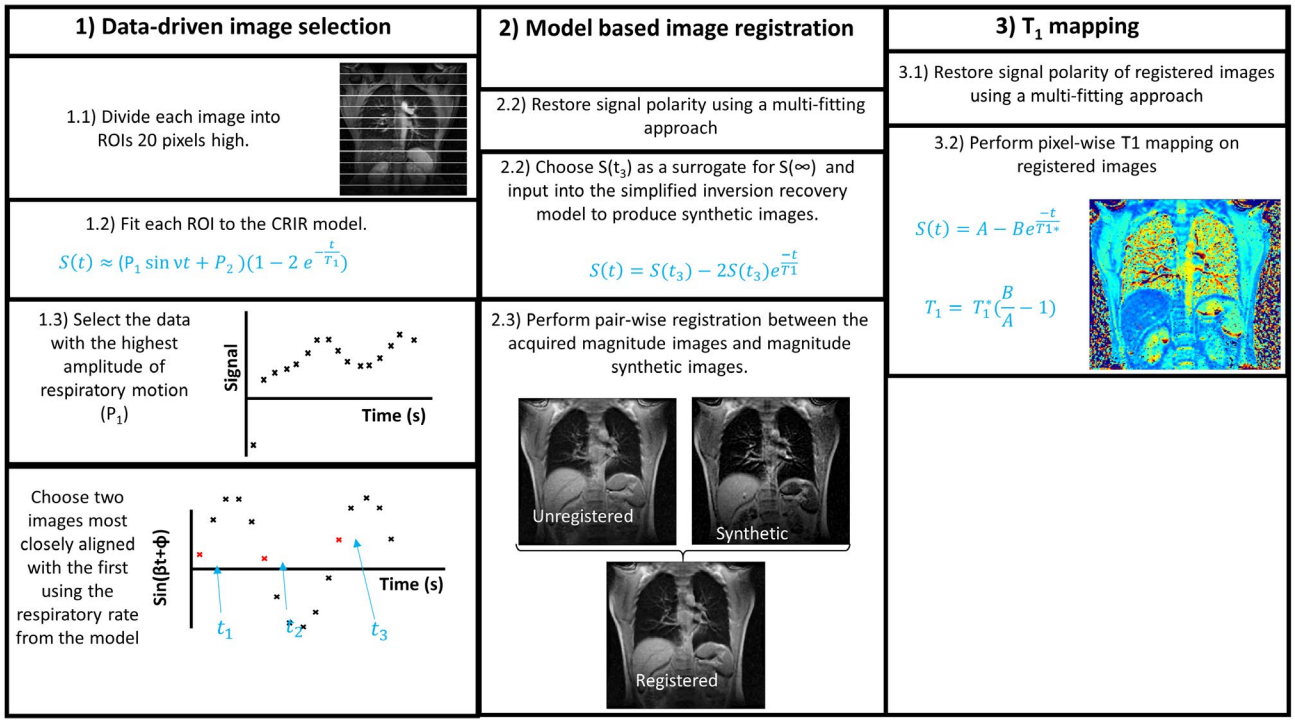


**FIGURE 1** Image registration and $T_1$ mapping process diagram. Data driven image selection is followed by model based image registration and $T_1$ mapping. (1) Data driven image selection: the image is split into horizontal ROIs (1.2). Mean signal at each time point is calculated from the ROIs, and is then fit to the CRIR model (1.3). After fitting, the respiratory rate and phase coefficients ($\nu$ and $P_2$ respectively) from the ROI with the highest amplitude ($P_1$) are selected. The $\nu$ and $P_2$ coefficients are then used to determine three images, which occur at a similar respiratory rate (1.4). (2) Model based image registration: Signal polarity is restored using a multi-fitting approach (2.2). The three images selected during the data driven image selection are then input into a simplified inversion recovery model to create synthetic images (2.2). The acquired images are then registered pair wise to the synthetic images (2.4). (3) $T_1$ mapping. After restoring signal polarity to the registered images using a multi-fitting approach (3.1), $T_1$ mapping is then performed (3.2).

and also any changes in the ratio of the different tissues (lung above diaphragm and abdominal tissue below diaphragm) in the ROI due to respiration (see Supporting Information Figure S1, which is available online. Curve fitting then determines the respiratory rate, $\nu$, which is subsequently used to select aligned images

## 2.2 | Combined respiratory and inversion recovery model derivation

The CRIR model predicts the mean signal of a ROI with a fixed position within the field of view (FOV) of the acquired images, see Supporting Information Figure S1. Within a given ROI, different tissues move in and out of the ROI due to respiration, causing the number of pixels ($n$), which correspond to a specific tissue within the ROI to change with time. If we consider two tissue compartments A and B that correspond for example to the lung and liver respectively, the inversion recovery signal from a ROI is given by:

$$S(t) = kn_A\rho_A\left(1-2e^{\left(-\frac{t}{T_{1A}}\right)}\right)+kn_B\rho_B\left(1-2e^{\left(-\frac{t}{T_{1B}}\right)}\right). \quad (3)$$

where $k$ is a constant, $n_A$ and $n_B$ are the number of pixels corresponding to tissue $A$ and tissue $B$ whose densities are $\rho_A$ and $\rho_B$ respectively.

During respiration the amount of pixels corresponding to tissue $A$ and tissue $B$ in the ROI will change. This can be approximated using a sinusoid:

$$n_A(t) = \propto \sin\left(\nu t+\emptyset_1\right)+\kappa_1 \quad (4)$$

$$n_B(t) = \beta \sin\left(\nu t+\emptyset_2\right)+\kappa_2. \quad (5)$$

where $\alpha$ and $\beta$ are the linear amplitude coefficients of the two periodic functions, $\kappa_1$ and $\kappa_2$ are constants, $\nu$ is the respiratory rate and $\Phi$ is the phase factor where $\emptyset_1$ and $\emptyset_2$ are out of phase by $\pi$. The $\pi$ phase shift between $\emptyset_1$ and $\emptyset_2$ occurs because the as tissue A increases, tissue B decreases such that tissue B is at a minimum when tissue A is at a maximum.

For simplicity in this model, it is assumed that changes to the relaxation times of the tissue compartments due to respiration ($T_{1A,B}$(t) and $T_{2A,B}$(t)) are much smaller than changes in the proportions of the specific tissues compartments in the ROI due to respiration and can, therefore, be neglected. Proton density may also change with time due to lung parenchyma compression and can be written as:

$$\rho_A = \rho_A(t) \quad (6)$$

$$\rho_B = \rho_B(t). \quad (7)$$

Therefore, Equations (4)-(7) can be substituted into Equation (3) to account for the movement of the tissues due to respiration, giving:

$$\begin{aligned} S(t) = {} & k\left(\propto\cos\left(\nu t+\emptyset_1\right)+\kappa_1\right)\rho_A(t)\left(1-2e^{\left(-\frac{t}{T_{1A}}\right)}\right) \\ & +k\left(\beta\sin\left(\nu t+\emptyset_2\right)+\kappa_2\right)\rho_B(t)\left(1-2e^{\left(-\frac{t}{T_{1B}}\right)}\right). \end{aligned} \quad (8)$$

Equation (8) can be further simplified by the assumption that the signal from the lung (tissue A) is much smaller than the signal from the tissue below the diaphragm, for example, liver (tissue B). In addition, it is assumed sub-diaphragmatic tissue is not compressed during respiration. Therefore:

$$S(t) \approx k\left(\beta\sin\left(\nu t+\emptyset_1\right)+\kappa_2\right)\rho_B(t)\left(1-2e^{\left(-\frac{t}{T_{1B}}\right)}\right) \quad (9)$$

which can then be rewritten as an equation with five free parameters:

$$S(t) \approx \left(P_1\sin\left(\nu t+\emptyset_1\right)+P_2\right)\left(1-2e^{\left(-\frac{t}{T_{1B}}\right)}\right). \quad (10)$$

This simplified model and its associated assumptions is set in place only for the purpose of selecting images for the construction of synthetic images as an intermediary for the improved spatial registration of the acquired images with different Ti.

# 3 | METHODS

## 3.1 | Subjects

All subjects were scanned with informed consent and ethical approval from the UK Research Ethics Committee. The 19 adult patients (mean age 70.3 ± 7 years, 74% male) with IPF were recruited from a specialist interstitial lung disease clinic, and 10 healthy volunteers (mean age 29.9 ± 5 years, 70% male) with no history of interstitial lung disease were recruited as controls. IPF was diagnosed based on an multidisciplinary team approach, and all IPF patients will have been diagnosed within 24 months of visit 1 MRI. All healthy volunteers and patients with IPF underwent 2D Look-Locker imaging in inspiration breath-hold, and during free breathing. About 8/19 patients and 8/10 healthy volunteers also underwent 2D Look-Locker imaging during breath-hold after expiration (approximately functional residual capacity). Ten patients with IPF also had 3D ultrashort echo time (UTE) imaging during the same examination. All patients had same-day pulmonary function tests and clinical CT data (acquired within the past 18 months) was also available.

Thirteen of the patients with IPF had follow-up 2D Look-Locker imaging during both breath-held inspiration and free breathing at 6 months after their initial MRI scan. All patients had same-day pulmonary function tests during follow-up.

One healthy volunteer (female, age 28) underwent multi-slice free breathing Look-Locker imaging to demonstrate the applicability of the technique to multi-slice acquisition. One healthy volunteer (male, age 34) also underwent 10 free-breathing, 10 inspiration breath-hold, and 10 expiration breath-hold Look-Locker acquisitions for repeatability testing, with the volunteer repositioned between repeated acquisitions.

## 3.2 | Pulmonary function tests

Forced vital capacity (FVC), carbon monoxide transfer factor (TLCO), and carbon monoxide transfer coefficient (KCO) were measured during pulmonary function tests on the same day as MRI. TLCO and KCO were calculated using the Global Lung Initiative (GLI) reference equations.[17]

## 3.3 | MRI acquisition parameters

A whole body 1.5T GE HDx scanner (GE Healthcare, Waukesha, WI) and eight-channel cardiac array coil were used for each 2D Look-Locker image acquisition. A coronal imaging slice was positioned through the descending aorta. The Look-Locker sequence comprises a global 180° inversion pulse followed by 16 gradient echo readout images.[9] Imaging parameters were as follows: inversion time (TI): 229 ms; repetition time (TR): 3.2 ms; TE: 0.9 ms; flip angle: 7°; phase × frequency: 128 × 128; slice thickness: 15 mm; pixel bandwidth: 244.14 kHz; FOV: 440 mm; overall acquisition time = 7 s. Breathing instructions for free breathing acquisitions were relaxed tidal breathing. 3D UTE imaging was performed using a radial gradient echo sequence with prospective gating on expiration.[18] TE/TR: 0.078/2.9 ms; flip angle: 4°; bandwidth 256 kHz; FOV: 400 mm. 60000 radial projections are acquired and matrix reconstructs to a 256 × 256 × 256 matrix resulting in a resolution of 1.56 isotropic.

## 3.4 | Synthetic image creation

Three images with close image alignment were determined using the CRIR parameters, $\nu$ and $\varphi$, and were input into the simplified inversion recovery model (Equation 10). The images were chosen automatically using an algorithm and correspond to the first image acquired and the subsequent two images that occur in the nearest respiratory state, determined by calculating the periodic term $\sin\left(\nu t+\emptyset\right)$ for each image. The condition that one of the latter two images must fall within the first seven acquired images is incorporated in order to ensure that the steep part of the inversion curve is effectively sampled for tissues with a short Ti.

The three input images were then fed into the one parameter simplified inversion recovery model, (see Equation 2), to create a set of spatially aligned synthetic images with similar contrast to the acquired images.

## 3.5 | Image registration

Image registration was performed using software[19] written in C and run from Matlab 2018. A diffeomorphic transformation was used, which was continuous and with one-to-one mapping. The similarity measure combines a sum of squares term and smoothing constraint, which reduces sensitivity to variations in signal intensity. If subjects did not successfully hold their breath during a breath-held scan, images also underwent image registration prior to $T_1$ mapping, using the same method. If a subject does not hold their breath, the effect of respiration on the signal will not be a simple sinusoid. Depending upon the response of the patient (ie, whether breath-hold is let go or drifts, and at what time during image acquisition) the signal might instead be better estimated using a combination of models. However, for this work the simple sine curve has been used. All images also then underwent successive image-to-image registration using the same registration software, for comparative purposes.

## 3.6 | Image analysis and statistics

After synthetic image creation, the magnitude data of all images were registered pairwise to their corresponding magnitude synthetic images. Signal polarity was restored using a conventional multi-fitting approach after image registration, following which $T_1$ maps are calculated using damped linear least squares curve fitting to:

$$S(t)=C-De^{-t/T_1^*} \tag{11}$$

with the Look-Locker $T_1$ correction:

$$T_1=T_1^*\left(\frac{D}{C}-1\right). \tag{12}$$

Lung $T_1$ was calculated by manually segmenting the two lungs, avoiding the heart and major blood vessels, and calculating an average of the right and left lung $T_1$ values. To assess the change in mean lung $T_1$ with

respiratory state, the difference between free breathing lung $T_1$ and inspiration breath-hold lung $T_1$ was calculated as: $\Delta T_{1(fb-insp)} = T_1\,(free\ breathing) - T_1\,(inspiration)$ Similarly, $\Delta T_{1(exp-insp)} = T_1\,(expiration) - T_1\,(inspiration)$ and $\Delta T_{1(exp-fb)} = T_1\,(expiration) - T_1\,(free\ breathing)$.

The image registration and $T_1$ mapping process was fully automated in Matlab on a 64 bit Windows 8.1 Pro workstation.

In patients who also underwent 3D UTE image acquisition during their MRI examination, a coronal slice through the descending aorta was identified from the 3D UTE images. The UTE image was used as a guide to draw ROIs on the $T_1$ maps in regions corresponding to fibrotic and non-fibrotic lung. Fibrotic and non-fibrotic lung ROIs were drawn at a similar height within the slice. Mean $T_1$ from fibrotic and non-fibrotic regions was calculated.

All statistical analysis was performed and presented using SPSS 24 (SPSS, Chicago, IL). Data are presented as mean ± SD. Box plots were presented as the median value the box representing interquartile range and the whiskers representing 1.5 × interquartile range. For intrasubject comparisons, Wilcoxon signed-rank tests were used to test differences between variables. For intersubject comparisons, Mann-Whitney U-tests were used.

### 3.7 | Image registration efficacy

For a qualitative assessment of motion, each set of breath-held images were rated based on a looping video of the acquired images. If the diaphragm did not appear to move across the images the breath-hold was considered successful, if the diaphragm did move across the images the breath-hold was considered unsuccessful. In the cases of unsuccessful breath-hold, images were categorized as either demonstrating diaphragmatic drift (a gradual drifting of the diaphragm position during the acquisition time) or a complete sudden release of breath-hold.

All acquired images (inspiration, expiration, and free breathing) were segmented manually using ITK-SNAP, including all of the lung including major vessels but excluding the heart itself if visible. Then the registration transformation from the corresponding image was applied to the segmentation.

Dice similarity coefficient (DSC) is a global alignment measurement and was calculated for each set of segmentations, before and after image registration:

$$DSC = \frac{2\ area\,(\boldsymbol{M} \cap \boldsymbol{N})}{area\,(\boldsymbol{M}) + area\,(\boldsymbol{N})}. \quad (13)$$

where $M$ and $N$ are two segmentations. DSC is calculated for each segmentation $M$, with respect to the reference segmentation, N. In this paper, DSC was averaged over all images, and over all images acting as segmentation $N$, see Equation (14). This is because no single image represents the ground truth of registration. The averaged DSC represents how well all images are aligned to all other images.

$$DSC = \sum_{i=1:16} \sum_{j=1:16} \frac{2\ area\left(\boldsymbol{M_i} \cap \boldsymbol{N_j}\right)}{area\left(\boldsymbol{M_i}\right) + area\left(\boldsymbol{N_j}\right)} \frac{1}{16 * 16} \quad (14)$$

where $i$ and $j$ are images acquired at different $Ti$. For breath-held acquisitions where additional registration was required, unregistered DSC was used for DSC comparisons.

## 4 | RESULTS

### 4.1 | Imaging feasibility

All healthy volunteers successfully held their breath during inspiration breath-hold scans, however two of eight healthy volunteers demonstrated diaphragm drift during expiration breath-hold scans. In patients with IPF, 9/19 did not successfully hold their breath during the inspiration acquisition (7/19 demonstrated diaphragm drift, 2/19 completely let go of breath-hold), and 4/8 did not successfully hold their breath during the expiration acquisition (2/8 demonstrated diaphragm drift, 2/8 completely let go of breath-hold).

Free breathing imaging was successful in all subjects and $T_1$ maps could be calculated successfully with the proposed approach in all subjects.

### 4.2 | Motion correction

After image-to-image registration free breathing DSC significantly decreased (unregistered DSC = 0.92 ± 0.03, registered DSC = 0.89 ± 0.03, $P < .001$) due to the registration errors introduced by the contrast differences between images, see Supporting Information Video S1.

DSC of free breathing images was significantly increased after image registration using synthetic images (registered DSC = 0.94, $P < .001$). In Figure 2, free breathing images before and after registration are presented, as well as plots of maximum inferior-superior lung length measured on each image in Matlab 2016b. All DSC data were skewed (unregistered inspiration DSC skewness: −1.8 ± 0.4;registered inspiration DSC skewness: −1.8 ± 0.4; unregistered expiration DSC skewness: 1.5 ± 0.06; registered expiration DSC skewness: −1.36 ± 0.4; registered free breathing DSC skewness: −0.97 ± 0.4).

Inspiration breath-hold DSC was significantly higher than registered free breathing DSC (inspiration DSC = 0.95

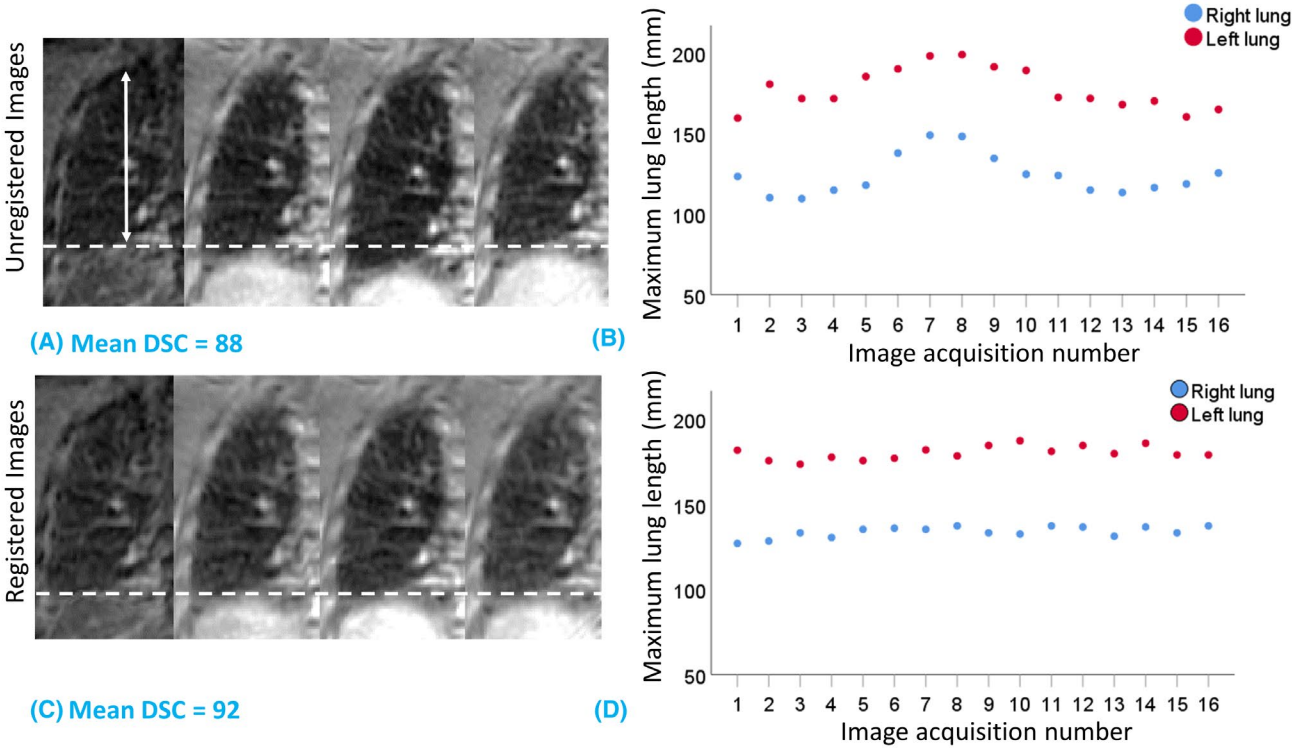


**FIGURE 2** Example of images from a patient with IPF. A, Shows time points 1, 6, 11, and 16 from the Look-Locker images before registration. B, Shows time points 1, 6, 11 and 16 from the Look-Locker images after registration using synthetic images. C, Lung length was measured from apex to base as shown by the white arrow. Lung length measured before registration was plotted for each time point. D, Lung length measured after registration was plotted for each time point. White dotted line reference line on (A) and (C) shows diaphragm position in image 1.

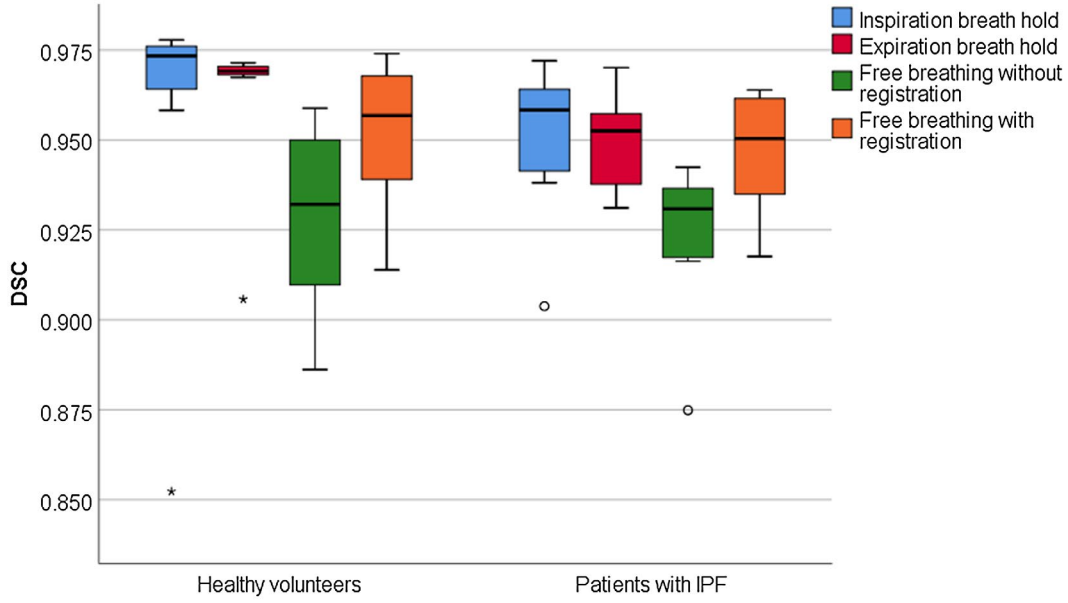


**FIGURE 3** Mean DSC for inspiration breath-hold, expiration breath-hold, and free breathing before and after image registration. Mean DSC for healthy volunteers was 0.96 ± 0.02 for inspiration breath-hold; 0.96 ± 0.02 for expiration breath-hold; 0.92 ± 0.03 for unregistered free breathing; and 0.95 ± 0.02 for registered free breathing. Mean DSC for patients with IPF was 0.95 ± 0.02 for inspiration breath-hold; 0.95 ± 0.02 for expiration breath-hold; 0.92 ± 0.02 for unregistered free breathing; and 0.95 ± 0.02 for registered free breathing. O denotes outliers, * denotes far outliers

± 0.03, registered free breathing DSC = 0.94 ± 0.02, $P$ = .007). There was no significant difference between expiration breath-hold DSC and registered free breathing DSC (expiration DSC = 0.95 ± 0.02, $P$ = .363). Figure 3 demonstrates box plots of the DSC for breath-hold and free breathing images in healthy volunteers and patients with IPF.

There was a small, but statistically significantly increase of DSC in inspiration breath-hold images after image registration using synthetic images (unregistered DSC = 0.95 ± 0.03, registered DSC = 0.95 ± 0.02, $P$ = .017). In the two cases where inspiration breath-hold was completely released during imaging, DSC increased from 0.94 ± 0.02 to 0.96 ± 0.01. Overall, there were no significant differences in DSC in expiration breath-hold images after registration using synthetic images (unregistered DSC = 0.95 ± 0.03, registered DSC = 0.95 ± 0.02, $P$ = .638). However, in the two cases where expiration breath-hold was let go, DSC increased from 0.931 ± 0.004 to 0.947 ± 0.005.

During multi-slice Look-Locker free-breathing imaging acquisition, full lung coverage was achieved with eight slices of thickness 15 mm in a total acquisition time of 56 seconds. The two most posterior slices showed poor image registration at the base of the lung, resulting in $T_1$ errors at the base of the lung in the corresponding $T_1$ maps. An example of a posterior slice and a central slice are shown in Supporting Information Video S2 to demonstrate this. The multi-slice T maps are presented with box plots representing mean and interquartile range of $T_1$ values for each slice in Figure 4.

## 4.3 | $T_1$

In healthy volunteers, lung $T_1$ was significantly higher during inspiration breath-hold when compared with expiration breath-hold (inspiration $T_1$ = 1.15 ± 0.09; expiration $T_1$ = 1.22 ± 0.10, $P$ = .018). These results are presented in Figure 5, and examples of $T_1$ maps in patients with IPF and healthy volunteers are shown in Figure 6. However, patients with IPF showed no significant difference in mean lung $T_1$ between the respiratory states imaged (inspiration $T_1$ = 1.11 ± 0.07, expiration $T_1$ = 1.15 ± 0.11, $P$ = .260), see Table 1.

The mean lung $T_1$ from the multi-slice free breathing Look-Locker acquisition was 1.21 ± 0.20 s, with a range of 1.01-1.41 s. Slices positioned in the middle of lung (slices 3-6) had a mean $T_1$ of 1.11 ± 0.19 s with a range of 1.01-1.23 s, see Figure 4. Lung $T_1$ repeatability was evaluated in one volunteer who underwent 10 image acquisitions in each of: inspiration breath-hold, expiration breath-hold, and during free breathing respectively. Inspiration breath-hold acquisitions resulted in a mean lung $T_1$ of 1.09 ± 0.04 s (range 1.04-1.16 s, mean whole lung SD of 0.24 ± 0.01 s), expiration breath-hold resulted in a mean lung $T_1$ of 1.14 ± 0.02 s (range 1.08-1.17 s, mean whole lung SD of 0.17 ± 0.01), and

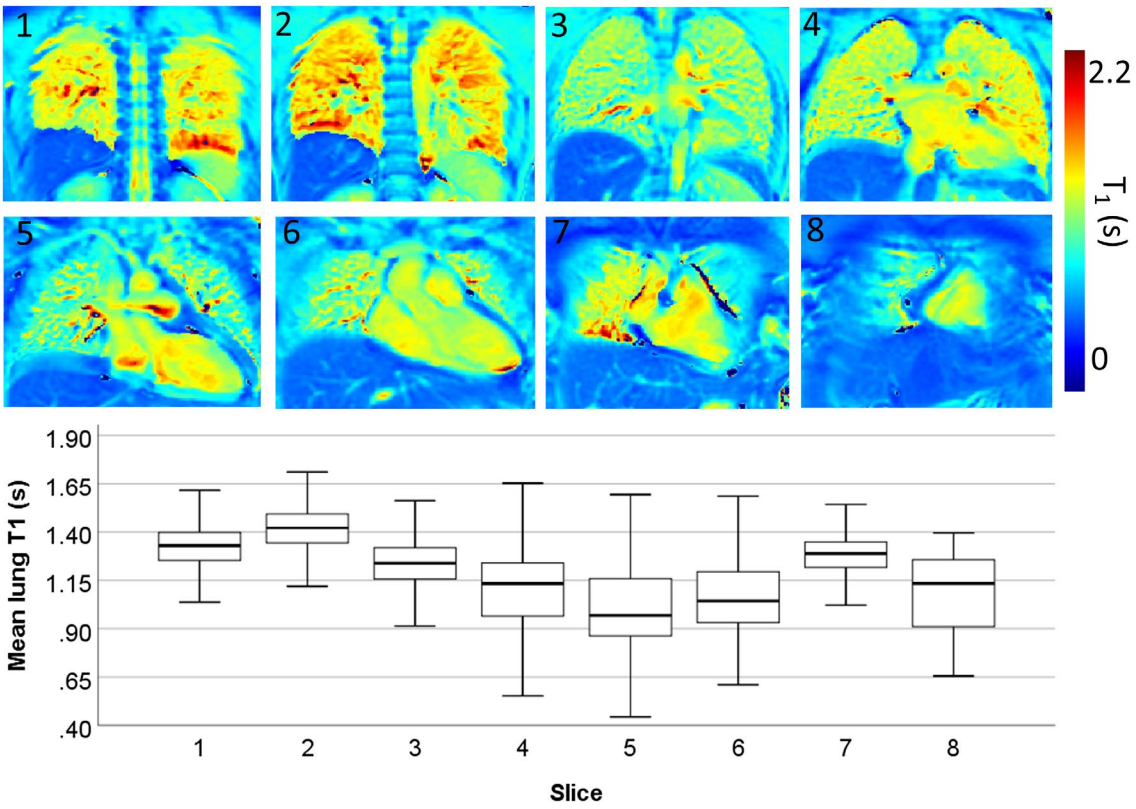


**FIGURE 4** Box plots showing the distribution of whole lung $T_1$ values from a multi-slice Look-Locker free-breathing imaging acquisition in a 28-year-old female volunteer. Mean lung $T_1$ for each slice was as follows: Slice 1 $T_1$ = 1.33 ± 0.13 s; slice 2 $T_1$ = 1.41 ± 0.13 s; slice 3 $T_1$ = 1.23 ± 0.16 s; slice 4 $T_1$ = 1.12 ± 0.19 s; slice 5 $T_1$ = 1.01 ± 0.20 s; slice 6 $T_1$ = 1.06 ± 0.19 s; slice 7 $T_1$ = 1.28 ± 0.13 s; slice 8 $T_1$ = 1.09 ± 0.19 s. Mean whole lung $T_1$ was 1.21 ± 0.2 s.

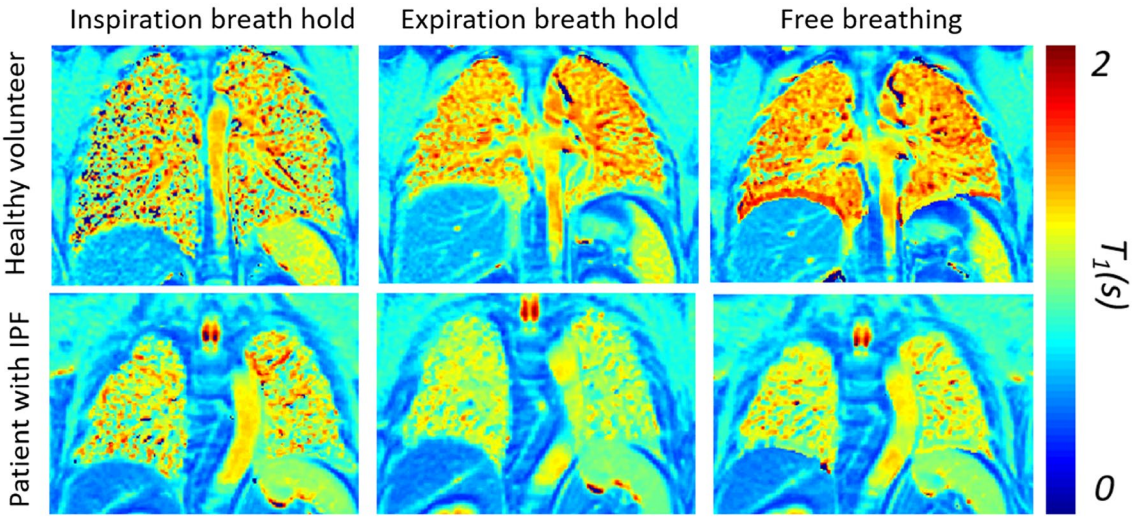


**FIGURE 5** Example $T_1$ maps in acquired during inspiration, expiration and free breathing in a healthy volunteer and a patient with IPF. At the base of the lung in both $T_1$ maps acquired during free breathing, a small amount of residual motion can be seen in the $T_1$ map. Where this has occurred, this area has been avoided when drawing ROIs.

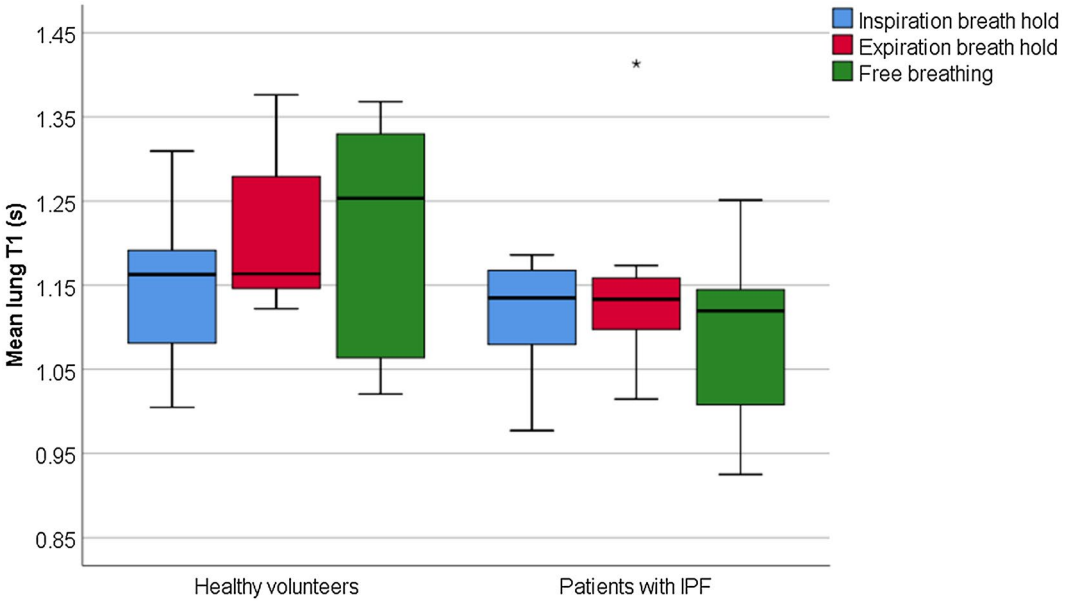


**FIGURE 6** Bar plot showing median $T_1$ values in volunteers and patients with IPF during inspiration breath, breath-hold, and during free breathing. There was a significant difference between free breathing $T_1$ values in healthy volunteers and patients with IPF, $P = .028$.

free breathing resulted in a mean lung $T_1$ of 1.12 ± 0.08 s (range: 1.02-1.24 s, mean whole lung SD of 0.19 ± 0.02). These results are presented in Figure 7.

$T_1$ was significantly lower in patients with IPF than in healthy volunteers when acquired during free breathing (healthy volunteers free breathing $T_1$ = 1.21 ± 0.14; patients with IPF free breathing $T_1$ = 1.08 ± 0.09, $P = .028$). $\Delta T_{1(fb-insp)}$, $\Delta T_{1(exp-fb)}$ and $\Delta T_{1(exp-insp)}$ were significantly different between healthy volunteers and patients with IPF ($P = .019$, $P = .015$ and $P = .015$ respectively). Intrasubject SD was significantly higher in patients with IPF than in healthy volunteers for $T_1$ maps acquired during inspiration breath-hold (healthy volunteers instrasubject SD = 0.22 ± 0.12 s, patients with IPF intrasubject SD = 0.25 ± 0.012, $P = .028$). There was not a significant difference in intrasubject SD of lung $T_1$ between patients with IPF and healthy volunteers for $T_1$ maps acquired during expiration (healthy volunteers instrasubject SD = 0.20 ± 0.02 s, patients with IPF intrasubject SD = 0.23 ± 0.1 s, $P = .343$) or free breathing (healthy volunteers intrasubject SD = 0.20 ± 0.01, patients with IPF intrasubject SD = 0.23 ± 0.1, $P = .086$), see Table 1.

**TABLE 1** $T_1$ data for images acquired during inspiration breath-hold, expiration breath-hold, and during free breathing in healthy volunteers and patients with IPF

| | Healthy volunteers | Patients with IPF | *P*-value for difference between healthy volunteers and patients with IPF |
|---|---|---|---|
| **Inspiration breath-hold** | | | |
| $T_1$ (s) | 1.15 ± 0.09 | 1.11 ± 0.07 | 0.233 |
| Intrasubject SD | 0.22 ± 0.12 | 0.25 ± 0.12 | 0.028* |
| Coefficient of variation (%) | 4.7 | 6.3 | |
| **Expiration breath-hold** | | | |
| $T_1$ (s) | 1.22 ± 0.10 | 1.15 ± 0.11 | 0.105 |
| Intrasubject SD | 0.20 ± 0.02 | 0.22 ± 0.02 | 0.343 |
| Coefficient of variation (%) | 8.2 | 9.6 | |
| **Registered free breathing** | | | |
| $T_1$ (s) | 1.21 ± 0.14 | 1.08 ± 0.09 | 0.028* |
| Intrasubject SD | 0.20 ± 0.01 | 0.23 ± 0.1 | 0.086 |
| Coefficient of variation (%) | 11.6 | 8.33 | |
| ***P*-values** | | | |
| *P* value between inspiration and expiration $T_1$ | 0.018[a] | 0.260[b] | - |
| *P* value between inspiration and free breathing $T_1$ | 0.059[a] | 0.161[b] | |
| *P* value between expiration and free breathing | 0.310[a] | 0.484[a] | |

*Note:* Due skewed data and low numbers, *P*-values for comparisons between inspiration, expiration and free breathing $T_1$ values were calculated using negative ranks or positive ranks. Comparisons between patients with IPF and healthy volunteered were made using Mann-Whitney U-tests.

[a]based on negative tanks.

[b]based on positive ranks.

*Indicates *P* value < .025;

**Indicates *P* value < .05.

UTE images from 6/10 patients showed fibrotic regions in the coronal slice through the descending aorta. In inspiration breath-hold $T_1$ maps, regions of fibrosis had a mean $T_1$ of 1.11 ± 0.10 s, regions without fibrosis had a mean $T_1$ of 1.13 ± 0.10 s, and the whole lung $T_1$ of these patients was 1.16 ± 0.03 s. In $T_1$ maps acquired during free breathing, regions of fibrosis had a mean $T_1$ of 1.14 ± 0.10 s, regions without fibrosis had a mean $T_1$ of 1.15 ± 0.10 and whole lung $T_1$ of 1.12 ± 0.07 s. Three of six patients with UTE images showing fibrotic regions also had expiration breath-hold $T_1$ maps. In expiration, fibrotic lung regions had a mean $T_1$ of 1.14 ± 0.10, regions without fibrosis had a $T_1$ of 1.13 ± 0.07 s and whole lung $T_1$ in those three patients was 1.14 ± 0.01 s. Figure 8 shows an example of region of interest placement on a UTE image in a patient with IPF, and corresponding breath-held and free breathing $T_1$ maps.

There was no difference in the intrasubject SD of $T_1$ values between expiration breath-hold and the free breathing acquisitions ($P = .433$); however, the intrasubject $T_1$ SD was significantly smaller in free breathing when compared with inspiration breath-hold.

Inspiration breath-hold lung $T_1$ was significantly higher in female volunteers when compared with males ($P = .022$); however, the trend in difference between males and females was seen in expiration or free breathing did not meet significance (expiration: $P = .053$; free breathing: $P = .079$). The mean lung $T_1$ in female healthy volunteers was 1.24 ± 0.06 s during inspiration, 1.32 ± 0.07 s during expiration and 1.30 ± 0.08 s during free breathing. The mean lung $T_1$ in male healthy volunteers was 1.11 ± 0.06 s during inspiration, 1.17 ± 0.07 s during expiration, and 1.17 ± 0.14 s during free breathing.

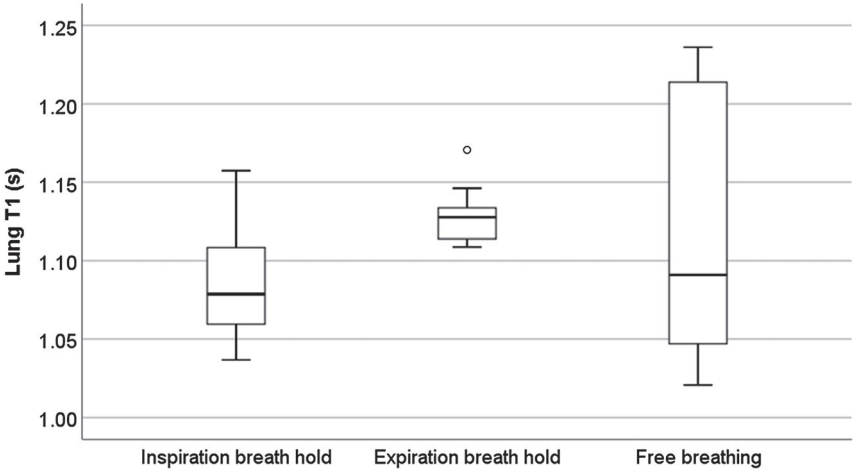


**FIGURE 7** Box plots demonstrating $T_1$ repeatability for inspiration breath-hold, expiration breath-hold and breathing acquisitions in a single healthy volunteer. All breath-holds were successfully held.

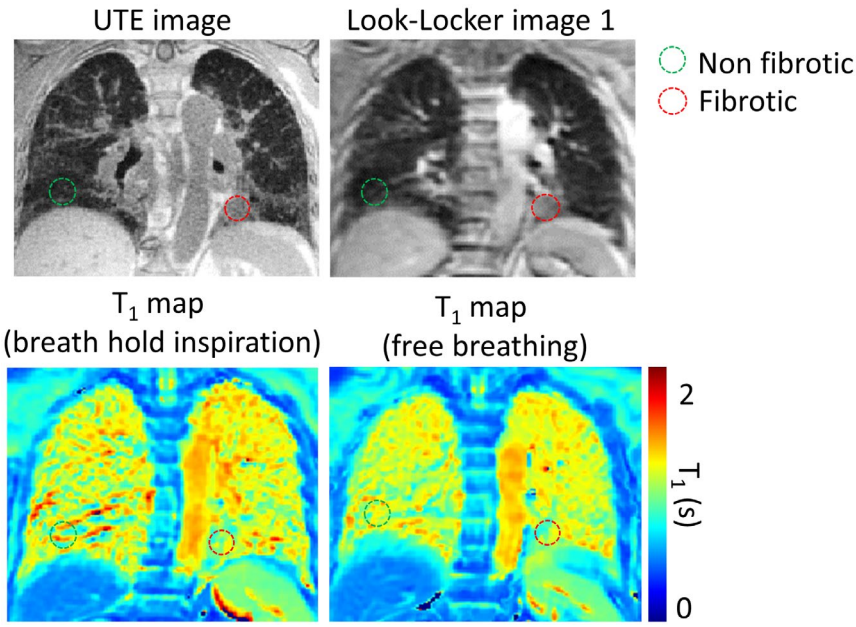


**FIGURE 8** Inspiration breath-hold and free breathing $T_1$ maps for a patient with IPF, and corresponding similar-slice UTE and Look-Locker image 1. Examples of the regions of interest drawn on the $T_1$ maps in areas which on the corresponding UTE image indicate fibrotic and non-fibrotic lung are shown. O denotes outliers.

In patients with IPF, there was no significant difference between male and female lung $T_1$ in any respiratory state (inspiration: $P = .784$; expiration: $P = .494$; free breathing $P = .441$). The mean lung $T_1$ in female patients with IPF was found to be 1.10 ± 0.08 s during inspiration, 1.11 s during expiration (n = 1) and 1.21 ± 0.07 s during free breathing. The mean lung $T_1$ in male patients with IPF was found to be 1.11 ± 0.06 s during inspiration, 1.12 ± 0.05 s during expiration and 1.09 ± 0.06 s during free breathing.

There was no significant correlation between age and lung $T_1$.

## 4.4 | PFTs

Patients with IPF had a mean forced expiratory volume in 1 s (FVC) of 87.6% of predicted volume, mean diffusing capacity of the lungs for carbon monoxide (TLCO) of 63.4% of predicted volume, and transfer coefficient of the lung for carbon monoxide (KCO) of 84.4%. Lung $T_1$ metrics did not significantly correlate with the % of predicted volume of FVC, TLCO, or KCO. Supporting Information Figure S2 shows example $T_1$ maps in a patient with IPF at visit 1 and visit 2. However, $\Delta T_{1(fb-insp)}$ did correlate with KCO (r = 0.480, $P$ = .044*) as did $\Delta T_{1(exp-insp)}$ (r = 0.872, $P$ = .010*), see Figure 9.

## 4.5 | Follow-up data

Mean lung $T_1$ was not significantly different at 6-mo follow-up when acquired during inspiration (visit 1: $T_1$ = 1.11 ± 0.08 s; visit 2: $T_1$ = 1.12 ± 0.05 s, $P$ = .597) or during free breathing (visit 1: $T_1$ = 1.09 ± 0.10 s; visit 2: $T_1$ = 1.14 ± 0.08 s, $P$ = .788). Mean FVC, TLCO, and KCO were also not significantly different at 6-mo follow-up (visit 1: FVC = 91 ± 17%, visit 2: FVC = 89 ± 15%, $P$ = .195; visit 1: TLCO = 65 ± 21%, visit

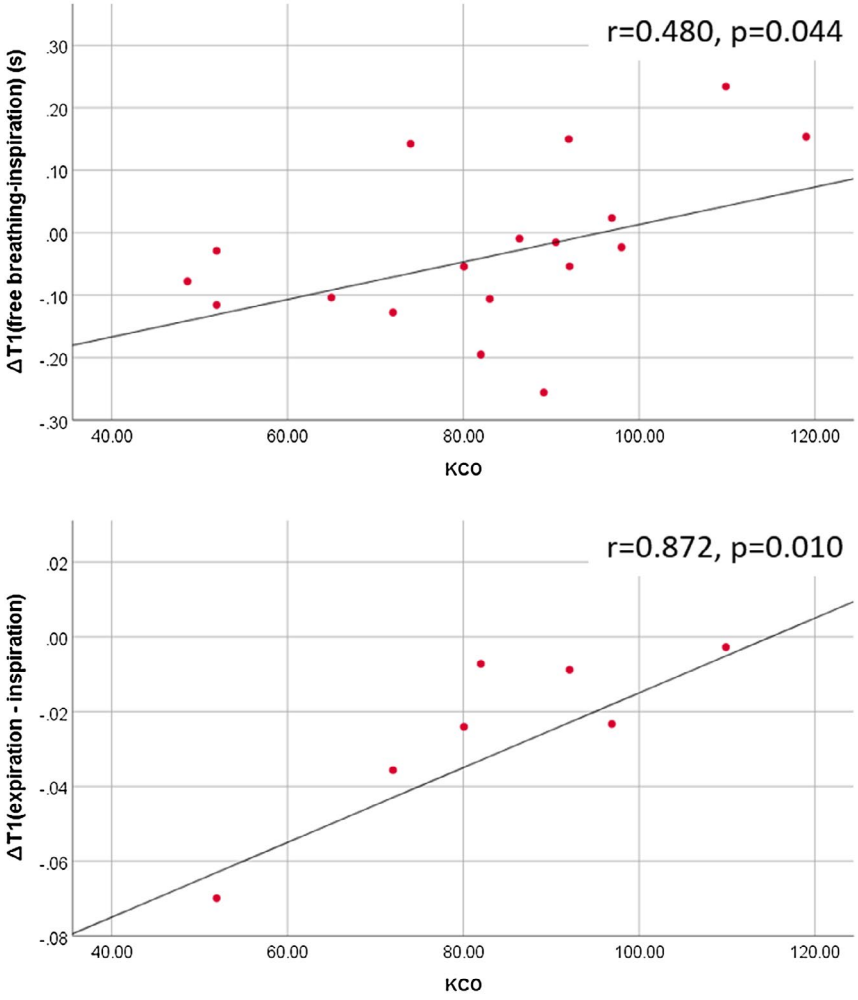


**FIGURE 9** Scatter plots showing KCO and change in $T_1$ between respiratory states, $\Delta T_{1(\text{fb-insp})}$ and $\Delta T_{1(\text{exp-insp})}$.

2: TLCO = 61.8 ± 26%, $P = .106$; visit 1: KCO = 84 ± 19%, visit 2: KCO = 81 ± 24%, $P = .182$).

## 5 | DISCUSSION

The presence of both diaphragm drift and the inability to maintain breath-hold in our IPF patient cohort suggests that free-breathing approaches may be a more comfortable and practical method of measuring lung $T_1$ in patients who experience shortness of breath. Image registration significantly improved the alignment of images acquired during free breathing and allowed multi-slice whole lung coverage in around 56 s. Evaluation of Look-Locker $T_1$ mapping repeatability in a single volunteer demonstrated the best repeatability with expiration acquisition (with breath-hold successful in all acquisitions) and the poorest repeatability with free breathing acquisition. The free breathing method proposed in this paper combines images from a range of lung inflation levels, and lung inflation level is known to affect measured $T_1$.[6] It may be that the combining of images acquired at different lung inflation levels has resulted in a less repeatable $T_1$ measurement.

The registration method presented also significantly increased image alignment in inspiration breath-hold images ($P = .018$). In particular, DSC increased after registration in all cases where breath-hold was completely released. Therefore, registration to synthetic images may also be useful in registering accidental motion in breath-held data.

The synthetic images are created from three images, and it cannot be guaranteed that the alignment between the three images input into the model are perfectly aligned, which may lead to some misalignment at the base of the lung where motion is most severe. The chances of identifying aligned images would be increased by acquiring multiple Look-Locker inversion recoveries and interleaving spatially aligned images, although there would be an associated scan-time cost.

The CRIR model assumes that lung density at the diaphragm is significantly lower than tissue density below the diaphragm, and this may not hold in the presence of severe lung fibrosis. In this study, DSC was significantly improved by the image registration method and mean DSC postregistration was higher in patients with IPF than healthy volunteers, indicating that the method works well in the presence of the fibrosis seen in the slices imaged

in these patients. Alternative methods to detect diaphragm position, for example, using deep learning, may be able to assist in this area.

MRI-based methods of tissue characterization are desirable as they do not expose patients to radiation. The implementation of MRI-based tissue characterization methods, such as late gadolinium enhanced inversion recovery MRI[20] and $T_2$ mapping[21] has been explored in patients with IPF. These methods also require breath-holds and may also be compatible with a synthetic-image based registration method, such as the one presented here but adapted for models of gadolinium uptake and $T_2$ recovery respectively. Additionally, as gated free-breathing acquisitions will have some amount of residual motion, the method also has the potential to be adapted to correct motion in gated acquisitions.

Although the majority of motion during respiration occurs within the coronal plane, smaller amounts of out-of-plane motion also occur during respiration, which have not been accounted for with this method. The 3D lung $T_1$ mapping, which registers motion in all directions, would resolve this problem and is a potential area for further work. This might be achieved using 3D or multi-slice free breathing acquisition and by calculating synthetic images with a common respiratory state for all slices.

Our findings are consistent with the work of Stadler et al[6] showing that lung $T_1$ is significantly higher in expiration than inspiration breath-hold in healthy volunteers[6]; however, in patients with IPF, this work did not find a significant difference between inspiration and expiration breath-hold $T_1$. The difference in lung $T_1$ due to respiratory state is likely to reflect a combination of changes that occur at different respiratory states, including significantly different lung perfusion,[22] lung density,[23] and in the case of breath-hold, blood oxygenation.[24] This work is not able to isolate the effects of these individual mechanisms that may contribute to the small but significant changes in lung $T_1$ with respiratory state and further work is warranted to identify these mechanisms. However, this work does indicate that the difference in $T_1$ between respiratory states may be of clinical interest in lung MRI of patients with IPF (as well as the lung $T_1$ values themselves). More work into this area with a greater number of patients is warranted.

Lung $T_1$ acquired during free breathing was found to be significantly lower in patients with IPF when compared with healthy volunteers, but was not found to be significantly lower using breath-hold manoeuvres. This indicates that free breathing $T_1$ imaging could be more sensitive to pathophysiological changes than breathold $T_1$ imaging. This could be due to sensitivity of the method to changes in lung inflation. Although all measures of mean lung $T_1$ were lower in patients with IPF when compared with healthy volunteers, only the lung $T_1$ acquired during free breathing was significantly different between the two groups. This is consistent with previous work by Stadler et al where two separate studies showed mean lung $T_1$ to be lower in patients with IPF than healthy volunteers.[1,6] The work of Mirsadraee et al has shown fibrotic lung regions to show a significantly higher $T_1$ than non-fibrotic lung regions at inspiration breath-hold at 3T using a MOLLI sequence.[2] The preliminary results in this work show a lower mean $T_1$ in fibrotic regions at inspiration breath-hold than the mean $T_1$ in non-fibrotic regions. However, due to small numbers the statistical significance of these preliminary reporting cannot be calculated. The differences between our preliminary reporting and the work of Mirsadraee et al may be due to the changes in $T_1$ values in fibrosis, lung tissue and blood with field strength and the fact that a MOLLI sequence was used. Further work characterizing the $T_1$ of fibrotic and non-fibrotic tissue is needed at both field strengths.

In healthy volunteers, lung $T_1$ was found to be significantly higher in females than in males ($P < .001$), which is consistent with previous findings.[25] Studies have shown that females have a higher blood $T_1$ than males.[26] This may be explained by lower hematocrit in women,[27] as decreased hematocrit levels increase blood $T_1$.[24] This work emphasizes the importance of gender being taken into account when evaluating lung $T_1$ changes.

PFTs did not indicate changes between visit 1 and visit 2. PFTs have been shown to have limited sensitivity in longitudinal assessment of IPF. Hyperpolarized gas MRI have shown to be sensitive to longitudinal changes in lung microstructure and gas exchange in patients with IPF in patients without significant changes in TLCO.[28] Therefore, due to the limited sensitivity of PFT measures, an absence of changes in PFTs does not necessarily indicate an absence of changes in the lung.

There was not a statistically significant longitudinal change in lung $T_1$ between visit 1 and visit 2. This may be due to a lack of change within the population, as indicated by the PFTs and the relatively short time-frame for follow-up assessments. Additionally, there were small patient numbers in the follow-up study.

## 6 | CONCLUSIONS

The use of spatially aligned synthetic images as an intermediary registration tool was successful in significantly reducing respiratory motion in free breathing acquisition of inversion recovery Look-Locker images. The resultant lung $T_1$ measured during a free breathing acquisition was significantly lower in patients with IPF when compared with healthy controls. The change in $T_1$ at different respiratory states, $\Delta T_{1(fb-insp)}$, $\Delta T_{1(exp-fb)}$ and $\Delta T_{1(exp-insp)}$, were also significantly different in patients with IPF when compared with healthy controls. The method proposed may improve the

robustness and clinical utility of lung $T_1$ mapping in patients who struggle to hold their breath.

## ACKNOWLEDGMENTS

The authors acknowledge Dr Kevin Johnson and Dr Fung Chan for their work on the UTE sequence used in this paper.

## ORCID

*Laura C. Saunders* https://orcid.org/0000-0002-1080-9861
*James A. Eaden* https://orcid.org/0000-0002-9314-7233
*Andrew J. Swift* https://orcid.org/0000-0002-8772-409X
*Jim M. Wild* https://orcid.org/0000-0002-7246-8660

## REFERENCES

1. Stadler A, Jakob PM, Griswold M, et al. T1 mapping of the entire lung parenchyma: Influence of respiratory phase and correlation to lung function test results in patients with diffuse lung disease. *Magn Reson Med*. 2008;59:96-101.
2. Mirsadraee S, et al. T1 characteristics of interstitial pulmonary fibrosis on 3T MRI-a predictor of early interstitial change? *Quant Imaging Med Surg*. 2016;6:42-49.
3. Jobst BJ, Triphan SMF, Sedlaczek O, et al. Functional lung MRI in chronic obstructive pulmonary disease: Comparison of T1 mapping, oxygen-enhanced T1 mapping and dynamic contrast enhanced perfusion. *PLoS One*. 2015;10:e0121520.
4. Maxien D, Dietrich O, Thieme SF, et al. Value of oxygen-enhanced MRI of the lungs in patients with pulmonary hypertension: A qualitative and quantitative approach. *J Magn Reson Imaging*. 2012;35:86-94.
5. Wells AU. Forced vital capacity as a primary end point in idiopathic pulmonary fibrosis treatment trials: MAKING a silk purse from a sow's ear. *Thorax*. 2013;68:309-310.
6. Stadler A, Jakob PM, Griswold M, et al. T1 mapping of the entire lung parenchyma: Influence of the respiratory phase in healthy individuals. *J Magn Reson Imaging*. 2005;21:759-764.
7. Gai ND, Malayeri AA, Bluemke DA. Three-dimensional T1 and T2* mapping of human lung parenchyma using interleaved saturation recovery with dual echo ultrashort echo time imaging (ITSR-DUTE). *J Magn Reson Imaging*. 2017;45:1097-1104.
8. Triphan SMF, Breuer FA, Gensler D, Kauczor HU, Jakob PM. Oxygen enhanced lung MRI by simultaneous measurement of T-1 and T-2* during free breathing using ultrashort TE. *J Magn Reson Imaging*. 2015;41:1708-1714.
9. Look DC, Locker DR. Time saving in measurement of NMR and EPR relaxation times. *Review of Scientific Intruments*. 1970;41:250-251.
10. Xue H, Shah S, Greiser A, et al. Motion correction for myocardial T1 mapping using image registration with synthetic image estimation. *Magn Reson Med*. 2012;67:1644-1655.
11. Tao Q, van der Tol P, Berendsen FF, Paiman EH, Lamb HJ, Van Der Geest RJ. Robust motion correction for myocardial T-1 and extracellular volume mapping by principle component analysis-based groupwise image registration. *J Magn Reson Imaging*. 2018;47:1397-1405.
12. Hayton P, Brady M, Tarassenko L, et al. Analysis of dynamic MR breast images using a model of contrast enhancement. *Med Image Anal*. 1997;1:207-224.
13. Hamy V, Dikaios N, Punwani S, et al. Respiratory motion correction in dynamic MRI using robust data decomposition registration—Application to DCE-MRI. *Med Image Anal*. 2014;18:301-313.
14. Melbourne A, Atkinson D, White MJ, et al. Registration of dynamic contrast-enhanced MRI using a progressive principal component registration (PPCR). *Phys Med Biol*. 2007;52:5147-5156.
15. Wollny G, Kellman P, Santos A, et al. Automatic motion compensation of free breathing acquired myocardial perfusion data by using independent component analysis. *Med Image Anal*. 2012;16:1015-1028.
16. Tilborghs S, Dresselaers T, Claus P, et al. Robust motion correction for cardiac T1 and ECV mapping using a T1 relaxation model approach. *Med Image Anal*. 2019;52:212-227.
17. Quanjer PH, Stanojevic S, Cole TJ, et al. Multi-ethnic reference values for spirometry for the 3–95-yr age range: The global lung function 2012 equations. *Eur Respir J*. 2012;40:1324-1343.
18. Johnson KM, Fain SB, Schiebler ML, et al. Optimized 3D ultrashort echo time pulmonary MRI. *Magn Reson Med*. 2013;70:1241-1250.
19. Barber DC, Hose DR. Automatic segmentation of medical images using image registration: Diagnostic and simulation applications. *J Med Eng Technol*. 2005;29:53-63.
20. Lavelle LP, Brady D, McEvoy S, et al. Pulmonary fibrosis: Tissue characterization using late-enhanced MRI compared with unenhanced anatomic high-resolution CT. *Diagnostic and Interventional Radiology*. 2017;23:106-111.
21. Buzan MTA, Eichinger M, Kreuter M, et al. T2 mapping of CT remodelling patterns in interstitial lung disease. *Eur Radiol*. 2015;25:3167-3174.
22. Cao JJ, Wang YI, Schapiro W, et al. Effects of respiratory cycle and body position on quantitative pulmonary perfusion by MRI. *J Magn Reson Imaging*. 2011;34:225-230.
23. Vandyk J, Keane TJ, Rider WD. Lung density as measured by computerized-tomography—Implications for radiotherapy. *Int J Radiat Oncol Biol Phys*. 1982;8:1363-1372.
24. Silvennoinen MJ, Kettunen MI, Kauppinen RA. Effects of hematocrit and oxygen saturation level on blood spin-lattice relaxation. *Magn Reson Med*. 2003;49:568-571.
25. Kindvall SSI, Diaz S, Svensson J, et al. Influence of age and sex on the longitudinal relaxation time, T1, of the lung in healthy never-smokers. *J Magn Reson Imaging*. 2016;43:1250-1257.
26. Reiter U, Reiter G, Dorr K, et al. Normal diastolic and systolic Myocardial T1 values at 1.5-T MR imaging: Correlations and blood normalization. *Radiology*. 2014;271:365-372.
27. Murphy WG. The sex difference in haemoglobin levels in adults—Mechanisms, causes, and consequences. *Blood Rev*. 2014;28:41-47.
28. Weatherley ND, Stewart NJ, Chan H-F, et al. Hyperpolarised xenon magnetic resonance spectroscopy for the longitudinal assessment of changes in gas diffusion in IPF. *Thorax*. 2019;74:500-502.

## SUPPORTING INFORMATION

Additional Supporting Information may be found online in the Supporting Information section.

**FIGURE S1** Diagram of a region of interest (ROI) with a fixed position within the FOV, with two tissues A and B moving in and out of the ROI

**FIGURE S2** Examples of $T_1$ maps from a patient at the initial assessment and 6-month follow-up, during free breathing and inspiration breath-hold

**VIDEO S1** Looping video of a healthy volunteer' Look-Locker images prior to registration (left), registered using image-to-image registration (middle) and registered using image to synthetic images (right) from a patient with IPF

**VIDEO S2** Looping video of Look-Locker images prior to registration (left) and registered using image to synthetic images (right) for two difference slice positions from a healthy volunteer

**How to cite this article:** Saunders LC, Eaden JA, Bianchi SM, Swift AJ, Wild JM. Free breathing lung $T_1$ mapping using image registration in patients with idiopathic pulmonary fibrosis. *Magn Reson Med*. 2020;00:1–15. https://doi.org/10.1002/mrm.28342